Bioactive Materials 6 (2021) 1107–1117

Contents lists available at ScienceDirect

Bioactive Materials

journal homepage: www.sciencedirect.com/journal/bioactive-materials

Nature-inspired topographies on hydroxyapatite surfaces regulate stem cells behaviour

Yogambha Ramaswamy [a,b,1], Iman Roohani [c,**,1], Young Jung No [a,b], Genevieve Madafiglio [a], Frank Chang [a], Furong Zhang [a], Zufu Lu [a,b], Hala Zreiqat [a,b,*]

[a] Biomaterials and Tissue Engineering Research Unit, School of Biomedical Engineering, University of Sydney, Sydney, NSW, 2006, Australia
[b] Australian Research Centre for Innovative BioEngineering, University of Sydney, Sydney, NSW, 2006, Australia
[c] School of Chemistry, Australian Centre for Nanomedicine, University of New South Wales, Sydney NSW, Australia

ARTICLE INFO

Keywords:
Stem cell
Biomaterials
Bioceramics
Scaffolds
Micropattern
Topography

ABSTRACT

Surface topography is one of the key factors in regulating interactions between materials and cells. While topographies presented to cells *in vivo* are non-symmetrical and in complex shapes, current fabrication techniques are limited to replicate these complex geometries. In this study, we developed a microcasting technique and successfully produced imprinted hydroxyapatite (HAp) surfaces with nature-inspired (honeycomb, pillars, and isolated islands) topographies. The *in vitro* biological performance of the developed non-symmetrical topographies was evaluated using adipose-derived stem cells (ADSCs). We demonstrated that ADSCs cultured on all HAp surfaces, except honeycomb patterns, presented well-defined stress fibers and expressed focal adhesion protein (paxillin) molecules. Isolated islands topographies significantly promoted osteogenic differentiation of ADSCs with increased alkaline phosphatase activity and upregulation of key osteogenic markers, compared to the other topographies and the control unmodified (flat) HAp surface. In contrast, honeycomb topographies hampered the ability of the ADSCs to proliferate and differentiate to the osteogenic lineage. This work presents a facile technique to imprint nature-derived topographies on the surface of bioceramics which opens up opportunities for the development of bioresponsive interfaces in tissue engineering and regenerative medicine.

1. Introduction

In nature, there are plants and animals with a wide variety of surface structures that are optimized to serve specialized functions. These structures have a large diversity in topographical shapes and varying degrees of surface roughness. They can also possess nano-to microscale hierarchy. These topographies are challenging to be fabricated by current manufacturing technologies and particularly to be made from inorganic materials [1–5]. Microcontact printing and micromachining are widely used to produce precisely controlled surface features, but these approaches require expensive equipment and still are limited to replicate intricate nature mimicked geometries. Lithographic based techniques are as well employed to create micropatterns on ceramic surfaces by using etching and high-energy beams. However, electron beams and lasers can induce phase changes, heat and/or chemical reactions to the underlying material [2]. Besides, lithography requires highly specialized and expensive equipment. The hydrothermal techniques are also employed to create complex topographies on the surface of ceramics using a reaction media and under high temperature and pressure [6–8]. However, these techniques are time-consuming and limited in controlling the size and shape of crystals that grow on the surface. It is well documented that topographical cues are instrumental in determining the outcome of cell-material interaction [9–12]. Considering that cells sense and respond to surface topographies, it is not surprising that these natural architectures can be an inspiration for tissue engineering applications. In this study, we aim to develop a ceramic microcasting technique to create nature-inspired surfaces to further explore the fascinating possibilities that nature offers by assessing the potential of these surfaces to control stem cell behaviour. To achieve the replication, an easy and straightforward procedure is

* Corresponding author. Biomaterials and Tissue Engineering Research Unit, School of Biomedical Engineering, University of Sydney, Sydney, NSW, 2006, Australia.
** Corresponding author.
E-mail addresses: iman.roohani@unsw.edu.au (I. Roohani), hala.zreiqat@sydney.edu.au (H. Zreiqat).
[1] These authors have contributed equally.

https://doi.org/10.1016/j.bioactmat.2020.10.001
Received 27 July 2020; Received in revised form 16 September 2020; Accepted 2 October 2020

carried out using a ceramic slurry containing hydroxyapatite (HAp) nanoparticles which subsequently cast into a mold containing the nature-derived template (petals or leaves).

In this study, we have successfully used the microcasting technique to develop a series of non-symmetrical nature-inspired topographies on HAp with three distinct shapes: (i) honeycomb (HC, complex form of pits with a mean depth of 12 μm, opening diameter of 18 μm and a basal diameter of 6 μm), (ii) pillar (PI, irregular form of protrusions with a mean height of 24 μm and, 34 μm spacing between the adjacent pillars), and isolated islands (IS, a scattered form of wells with a mean depth of 5 μm, and width of 12 μm). The influence of these patterned on the behaviour of ADSCs and their osteogenic differentiation potential are evaluated.

2. Materials and methods

2.1. Fabrication of HAp powder and preparation of slurry

HAp is an osteoconductive and osteogenic bioceramic that has a long history in bone tissue engineering applications and synthesized using a variety of techniques [13,14]. The spherical HAp nanoparticles with d_{50} = 30 nm were synthesized according to the previously published paper [15]. Briefly, ammonium phosphate dibasic (Product No: 09839, Sigma-Aldrich) solution was added dropwise to calcium nitrate solution (Product No: C1396, Sigma-Aldrich), at a temperature of 70 °C and keeping pH 8.4 by addition of ammonia solution. The obtained precipitates were washed several times with Milli-Q (MQ) water and subsequently dried in an oven overnight at 80 °C. To prepare the ceramic slurry, 1 g of Darvan 811 (CeramicShop, USA) was dissolved in 20 mL MQ water. After complete dissolution of Darvan 811, 0.5 mL of 1 wt% Hydroxypropyl methylcellulose ((HPMC) Methocel F4M, Dow Chemical) solution added to the Darvan solution. HAp (100 g) was slowly added to the HPMC-Darvan solution under continuous stirring for 2 h. The obtained mixture was homogenized by a centrifuge mixer (Thinky Mixer, ARE-250, Japan) for 10 min at 1500 rpm. To remove agglomerates, the slurry was transferred to a 500 mL zirconia jar and milled at 150 rpm for 2 h by a planetary ball mill (Retsch PM400, Germany). After the deagglomeration process, the slurry was packed into 50 mL syringes.

2.2. Patterning of HAp ceramics

We chose the petals with flat, undamaged, and clean surface then gently dip the petals in MQ-water and blotted their surface. As shown in Fig. 1, a flat region of a parsley (*Petroselinum crispum*) or rose (*Rosa kordesii*), or daisy (*Orchidaceae)* leaf or petal was selected and cut by a scalpel blade, then placed on a glass slide and secured with the help of a silicon ring. A sealant was used to act as a support for blocking the backside from slurry leakage. The slurry was injected into the mold and spread over the leaf by gently tapping the glass slide. The samples were kept at the room temperature for 24 h to dry. After drying, leaves were carefully peeled off and disks were sintered at 1200 °C for 3 h with a heating rate of 5 °C.min^{-1} in a furnace (Carbolite, Germany). A debinding step was not necessary for the thermal cycle due to low

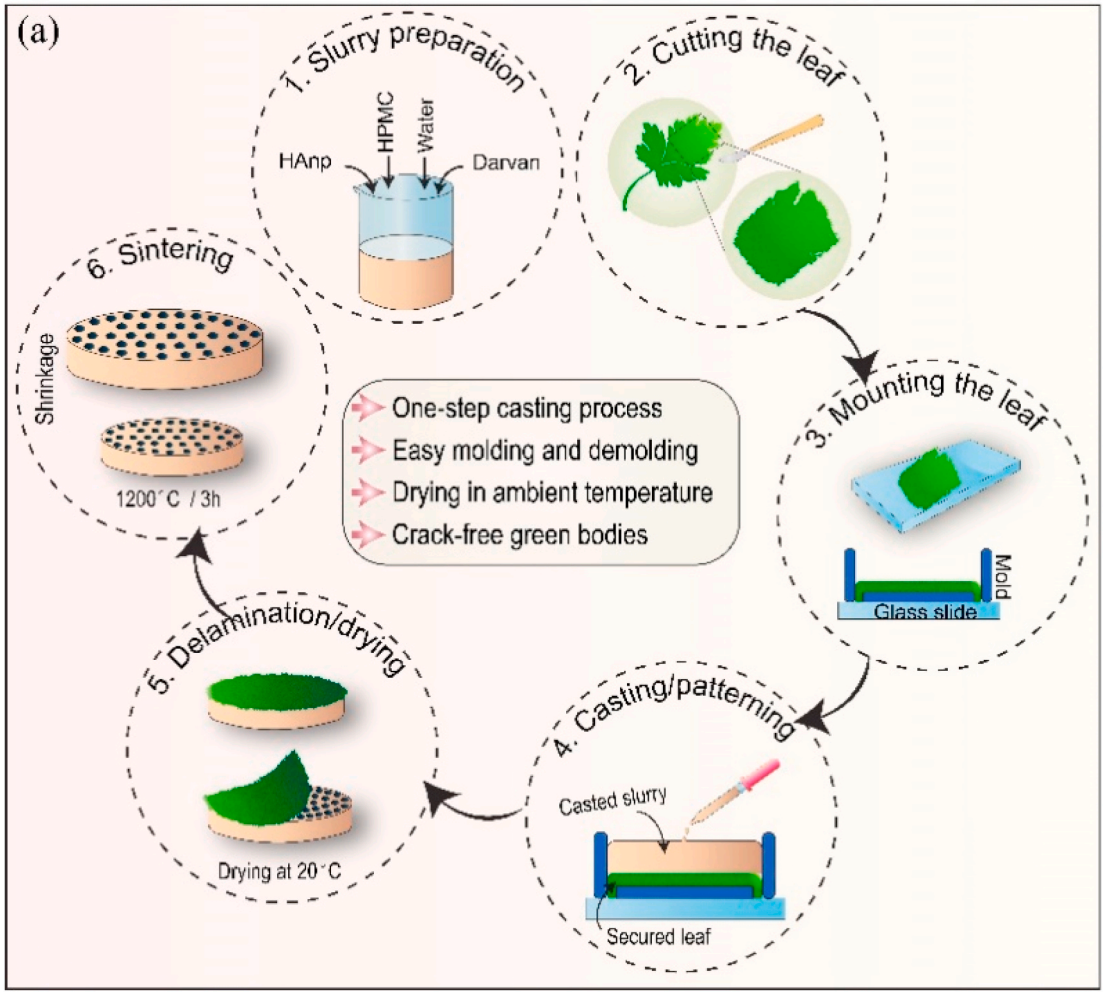

Fig. 1. Schematic diagram of the processes involved in the fabrication of micropatterned HAp ceramics by a microcasting technique using natural plant surfaces.

amount of organic component. After sintering, disks were cleaned using sonication in undenatured ethanol. For the preparation of control groups, slurries were cast on a silicon film and then sintered disks were ground by using a series of sandpapers and finally polished with diamond paste to obtain a mirror finish surface. Flat (FL) substrate was used as a control material and three distinct patterns were developed such as "honeycomb" (HC), "pillars" (PI) and "isolated island" (IS). Fig. S1 depicts nature-inspired topographies in a myriad of shapes and sizes using the microcasting technique.

2.3. Characterization of sintered HAp ceramics

The phase chemical composition of sintered disks was identified by X-ray diffraction analysis (XRD, Shimadzu S6000) (Fig. S2). The patterned ceramic surfaces were imaged by scanning electron microscopy (UltraPlus, Zeiss, Field emission, Germany). The pattern height, width and length were determined by using image analysis software (ImageJ) on the SEM images. For measurement of pattern depth, samples were mounted in resin and then cut by a diamond saw, and the cross-sections were subsequently analyzed by SEM.

2.4. ADSCs attachment on patterned HAp substrates

Human adipose-derived stem cells (ADSCs) were purchased from the Invitrogen Technologies and the cells from three donors were mixed and expanded to reach passage four by culturing in MesenPRO basal medium with 2 mM L-glutamine and MesenPRO RS Growth Supplement (Invitrogen). Passage 4 ADSCs were used for all the experiments. The attachment of ADSCs cultured for 24 h on the ceramic disks was analyzed using scanning electron microscopy. Briefly, the ADSCs were seeded on the disks at the density of 10,000 cells per mL and cultured for 24 h in growth medium consisting of α-minimal essential medium (α-MEM, Gibco Laboratories), supplemented with 10% (v/v) foetal calf serum (Gibco Laboratories), 100 U/mL penicillin, and 100 mg/mL streptomycin (Gibco Laboratories). After 24 h of culture, cells were rinsed in phosphate-buffered solution (PBS), fixed in 1.25% glutaraldehyde and sequentially dehydrated in graded ethanol. Samples were dried in hexamethyldisilazane and coated with gold for scanning electron microscopy (SEM) analysis using FE-scanning electron microscopy (Zeiss Ultra).

2.5. Paxillin/actin staining and confocal microscopy

ADSCs were cultured on all the HAp substrates at the density of 10,000 cells/mL for 2 and 24 h to examine the expression of paxillin and the actin stress fibres. At the end of each time point, the cells were fixed in 4% paraformaldehyde for 30 min and washed in PBS and then permeabilized with 0.2% Triton-X, blocked in PBS (5% bovine serum albumin (BSA)). The cells cultured for 24 h was washed and incubated with primary antibody (*anti*-Paxillin) for 1 h at room temperature (RT). Cells were then washed in PBS three times and incubated with the secondary antibody (α-mouse-Alexa 488 (A11029, Invitrogen) and 120 ng/mL TRITC-conjugated Phalloidin for 1 h at RT. Nuclei were stained with DAPI (1/1000) for 10 min and thoroughly washed in 0.05% Tween in PBS. The cells cultured for 2 h on all the HAp substrates were stained only with TRITC-conjugated Phalloidin for 1 h at RT. Prolong gold antifade reagent was applied before imaging them using a Leica SL100 confocal microscope.

2.6. Proliferation of ADSCs on HAp ceramic substrates

The proliferation of ADSCs was quantitatively assessed by MTS (3-(4,5-dimethylthiazol-2-yl)-2,5-diphenyltetrazolium bromide) assay after 1, 3 and 7 days of culturing 40,000 cells/mL in growth media on all HAp substrates. 100 μL of the reacted reagent from each well was transferred to 96-well plate at the end of each time point and the absorbance was recorded using a microplate reader at the wavelength of 490 nm.

2.7. Alkaline phosphatase activity of ADSC on the patterned HAp

The differentiation of ADSCs cultured on all the HAp substrates was assessed by measuring the ALP activity using *p*-nitrophenyl phosphate substrate as described previously [16]. ADSCs were plated at a concentration of 30,000 cells per disk in a 24 well plate and cultured in osteogenic differentiating medium (Invitrogen, StemPro™, A1007201) for 7 and 14 days. At the end of each time point, cells were washed gently three times in PBS followed by washing once in cold 50 mM Tris buffer, before lysing in Tris buffer containing 0.2%NP-40 solution. 2 mL of the lysate was then added to 100 mL of *p*-nitrophenol phosphate (ThermoFisher, USA) in a 96-well plate and incubated for 30 min at 37 °C. The reaction was stopped using 100 mL of 0.1 N NaOH and the absorbance was recorded using spectrophotometry (405 nm). The ALP activity was calculated from a standard curve after normalizing to the total protein content, using a Pierce BCA Protein Assay Kit.

2.8. Quantitative real-time polymerase chain reaction

Total RNA was isolated from ADSCs cultured on all the HAp ceramic disks using the Rneasy Mini Kit from Qiagen (Valencia, CA, USA) according to the manufacturer's instructions. First-strand cDNA was synthesized from 1 μg total RNA using the Omniscript RT kit (Qiagen) according to the manufacturer's instructions. Quantitative reverse transcription polymerase chain reaction (RT-PCR) was performed to analyse the osteogenic differentiation of ADSCs. The RNA from the ADSCs, seeded at a concentration of 100,000 cells per mL was extracted at day 4 and day 14. It was then analyzed for the expression of osteogenic markers such as collagen type 1 (COL 1), alkaline phosphatase (ALP), osteopontin (OPN), runt-related transcription factor 2 (RUNX-2) and bone morphogenetic protein 2 (BMP-2) using a rotor-gene 6000 (Corbett Life Science). Relative gene expression was normalized with the house-keeping gene 18 S and the primers for the selected genes are listed in Table 1.

2.9. Protein extraction and western blot analysis

ADSCs were cultured for three days on all the HAp substrates and at day 3 the substrates were washed with ice-cold PBS, lysed for 30 min in ice-cold Radio Immuno Precipitation Assay lysis buffer (Sigma, St. Louis, MO, USA), and phosphatase inhibitor (Roche). Protein concentration was measured using the BCA protein assay kit (Pierce). 10 μg protein samples in 4× sample buffer (WesternBreeze, Invitrogen) were heated at 70 °C for 10 min and separated on 8%–12% sodium dodecyl sulphate

Table 1
List of primers for osteogenic markers used for RT-PCR –Shown are the details of the primers used for RT-PCR, including annealing temperatures, and forward (F) and reverse I sequences. 18 S; COL1; OPN; ALP; RUNX-2; BMP-2.

	Sequence (5′–3′)	Annealing temperature (oC)
18S	F GTAACCCGTTGAACCCCATT R CCATCCAATCGGTAGTAGCG	60
Col 1	F AGGGTCCCAACGAGATCGAGATCCG R TACAGGAAGCAGACAGGGCCAACGTCG	60
OPN	F TTCCAAGTAAGTCCAACGAAAG R GTGACCAGTTCATCAGATTCAT	60
ALP	F CGTGGCTAAGAATGTCATCATGTT R AGGGGAACTTGTCCATCTCC	60
RUNX-2	F ATGCTTCATTCGCCTCAC R ACTGCTTGCAGCCTTAAAT	60
BMP-2	F AGTTGCGGCTGCTCAGCATGTT R CCGGGTTGTTTTCCCACT	60

(SDS)-polyacrylamide electrophoresis gels (WesternBreeze, Invitrogen). Proteins were transferred to the polyvinylidene fluoride (PVDF) membrane and washed with Tris buffer solution (20 mM Tris-HCl, pH 7.6 and 137 mM NaCl) containing 0.1% Tween 20. The membrane was then blocked for 1 h at RT in Tris –Tween buffer with 1% bovine serum albumin (BSA). After blocking, the membrane was washed three times and incubated in primary antibodies, *anti*-BMP2 (Abcam, 1:1000), *anti*-Smad1 (Cell signalling, 1:1000) or *anti*-phospho-Smad1/5 (*p*-Smad1/5, Cell signalling, 1:500) and β-actin (1:5000, Abcam) as a loading control, in blocking buffer on the shaker at 4 °C overnight. Following three washes, the membrane was incubated in the secondary antibody conjugated with alkaline phosphatase (WesternBreeze, Invitrogen) for 1 h at RT. Chemiluminescent reagent (WesternBreeze, Invitrogen) was used to observe the protein bands under the Bio-Rad ChemiDoc MP Imaging System (Bio-Rad).

2.10. Statistical analysis

All data were expressed as mean ± standard deviation (SD) and were analyzed using one-way ANOVA, p-value < 0.05 was considered to be statistically significant. In figures, "*" indicates a p-value <0.05 versus the control, flat HAp disks (FL).

3. Results

3.1. Successful imprinting of nature-derived patterns on HAp

Fig. 2a and b shows the nature-inspired patterns including *Petroselinum crispum* (for IS), *Orchidaceae* (for PI) and *Rosa kordesii* (for HC) and respective generated HAp surfaces, after sintering for each pattern. We assessed the quality of topographies on disks and observed that topographies had a consistent size and distribution. The size distribution of each topography was quantified by ImageJ (Fig. 2c). For the IS, the mean depth of channels was 5.1 ± 0.8 μm, each channel was 12.5 ± 1.8 μm wide, and each set of these islands bounded by a continuous wall was 41.2 ± 5.5 μm wide. For the pillars, the mean height of the pillars was 24.0 ± 8.0 μm, the base and tip of the pillars were 29.6 ± 8.6 μm and 12.7 ± 4.3 μm respectively, and the mean distance from each pillar from centre-to-centre was 33.8 ± 11.1 μm. Honeycomb structures characterized by circular pits separated by a thin wall, the pits had a mean depth of 11.9 ± 2.1 μm, the opening and basal diameters of the pits were 18.5 ± 3.6 μm and 6.3 ± 1.3 μm respectively. The thickness of the walls between the pits was 1.5 ± 0.4 μm.

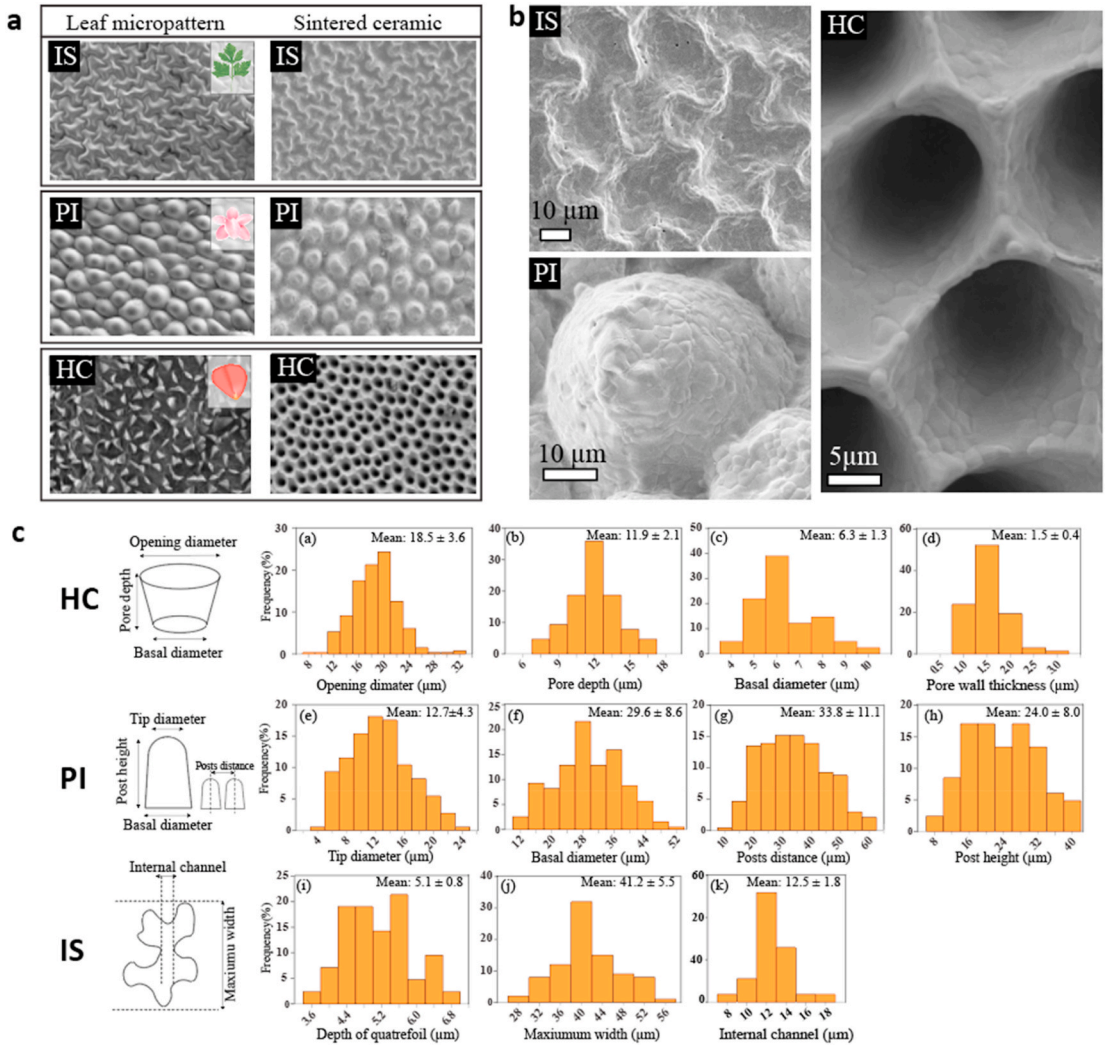

Fig. 2. (a) Scanning electron microscopy images of the plant surfaces and corresponding replicated topographies, isolated islands (IS), pillars (PI), and honeycomb (HC) on HAp disks. (b) High magnification images of IS, PI, and HC demonstrate the efficacy of the microcasting technique in the replication of intricate structures of natural plants. (C) Distribution profiles of dimensions for topographies: (a–d) HC, (e–h) PI, and (i–k) IS measured by image analysis of SEM micrographs. Data are shown as mean ± standard deviation, all measurements are in μm.

3.2. Adhesion of ADSCs on the patterned HAp substrates

SEM results demonstrated marked variations in the morphology of the adhered ADSCs on HAp disks. On FL and the IS, ADSCs spread and exhibited flattened morphologies (Fig. 3a and d) with distinct filopodia. In contrast, ADSCs on the HC and PI substrates resumed an elongated morphology with reduced cell protrusions, compared to those seen on the IS and the control FL surfaces with cell-cell contact maintained between the groves of the substrates (Fig. 3b and c).

3.3. Cytoskeletal organization and expression of focal adhesion molecule

Phalloidin and paxillin staining were carried out to determine the effect of all HAp surfaces on the cytoskeletal organization and the expression of focal adhesion molecule by ADSCs. ADSCs cultured on the HAp substrates for 2 h showed a rounded morphology (Fig. S3). However, after 24 h the cytoskeletal organization of the cells varied distinctively (Fig. 4a). ADSCs attached on IS and FL maintained cell-cell contacts and exhibited numerous well defined and organized intersecting actin microfilaments. On the PI, cells were more elongated and were not able to express the actin filaments as distinctively as the control (FL) or IS. ADSCs on the HC remained largely rounded or formed cell clusters unable to exhibit any organized actin filaments (Fig. 4a). Paxillin-containing adhesion junctions were chosen as an overall structural marker of focal adhesions. ADSCs cultured on IS showed regions of strong paxillin expression around the periphery of the cells as compared to the FL or the PI substrates and no such explicit expression was observed on HC substrates (Fig. 4b).

3.4. Proliferation of ADSCs on the patterned HAp

The proliferation of ADSCs on the patterned substrates was examined using the MTS assay. ADSCs were able to proliferate progressively with time on all the substrates. However, by day 7 cell proliferation was significantly higher on the PI and IS compared to the control (FL). In the case of HC, cells were able to proliferate but they were significantly lower than the FL substrates (Fig. 5a).

3.5. Differentiation of ADSCs on the HAp substrates: alkaline phosphatase activity

ADSCs were seeded on all the HAp substrates and the differentiation under osteogenic conditions was determined by the ALP activity on day 7 and day 14. Quantitative analysis revealed that on day 7, ALP activity of the cells grown on PI substrates was significantly higher compared to the FL substrates. On day 14, there were substantial differences in the ALP activity on IS and PI with both substrates showing a significant increase compared to the FL substrates. However, on the HC, the level of ALP activity was significantly decreased compared to FL (Fig. 5b).

3.6. Differentiation of ADSCs on the HAp substrates: osteogenic gene expression

The osteogenic differentiation of ADSCs on all the HAp substrates was determined by the expression levels of osteogenic genes. Real-time PCR was used to examine the mRNA expression levels for COL1, RUNX-2, ALP and OPN at day 4 and day 14 (Fig. 6a–d). It was observed that by day 14 the expression of COL1 was significantly upregulated on IS compared to the FL substrates. Similarly, ADSCs seeded on PI and IS showed a significant upregulation in the expression of RUNX-2 as compared to the FL substrates on both day 4 and day 14. ALP mRNA expression levels on FL substrates was significantly higher than the IS at the initial time point of day 4. However, by day 14 the expression of ALP was significantly upregulated on IS compared to PI or FL substrates. Expression of OPN was also upregulated on PI and IS on both days 4 and 14 as compared to FL. Although the expression levels of all the genes were upregulated on HC between day 4 and day 14; this effect was significantly lower compared to the other substrates (FL, PI and IS).

3.7. BMP/smad signalling pathway

BMP/smad signalling pathways play critical roles in the regulation of

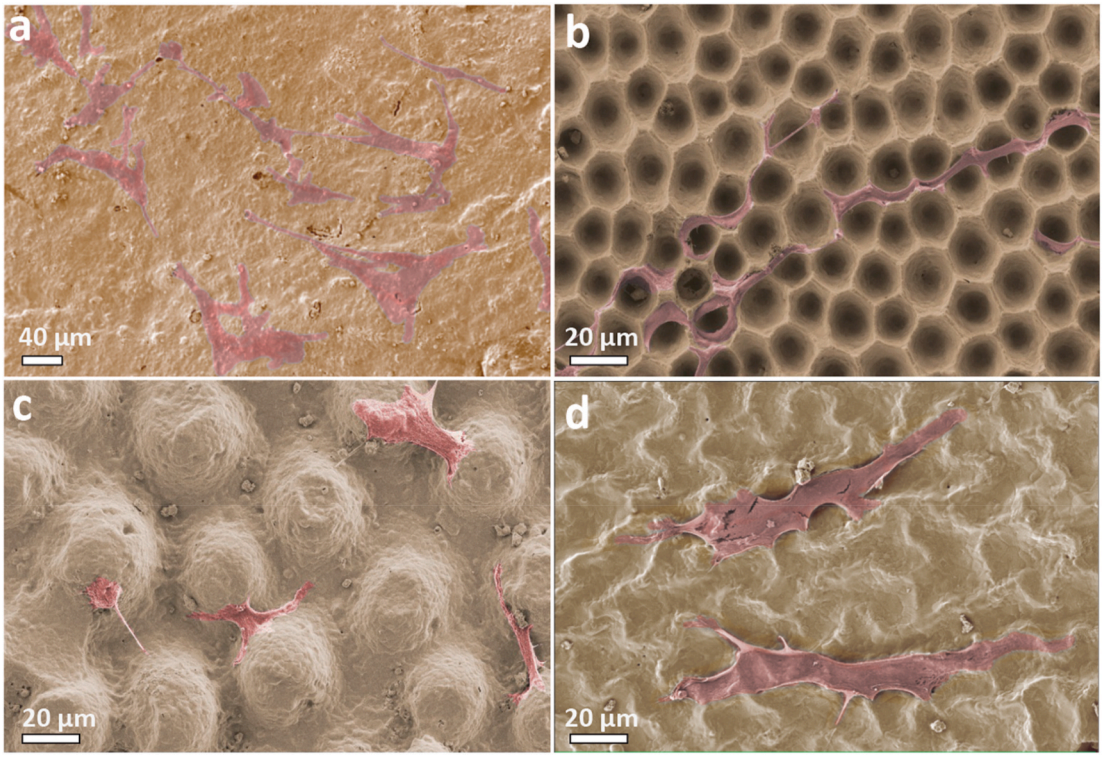

Fig. 3. False-colored SEM images of the ADSCs attached on HAp disks: (a) FL, (b) HC, (c) PI and (d) IS after 1 day.

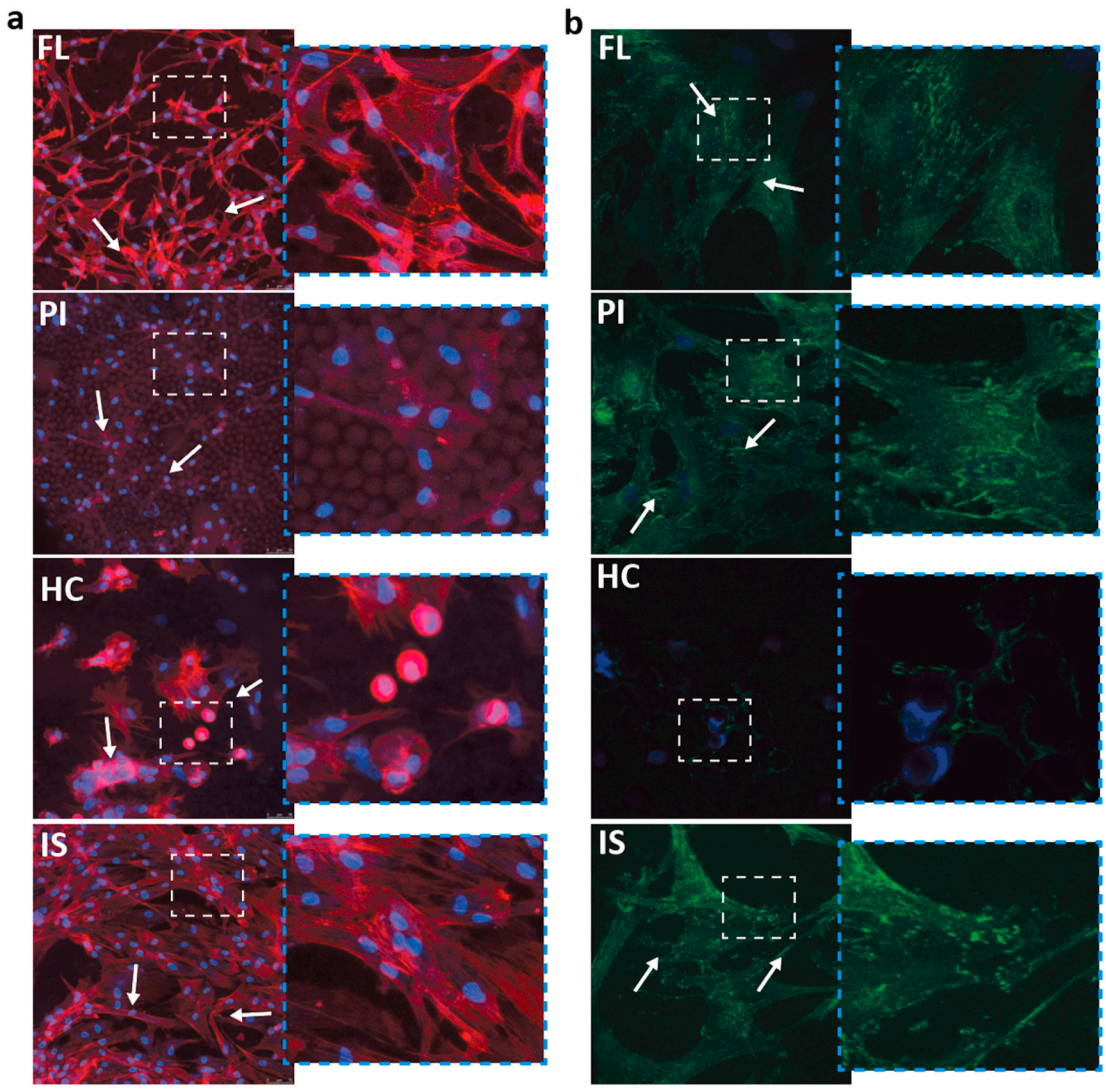

Fig. 4. Confocal microscopy images (a) Cytoskeleton organization of the ADSCs cultured for 24 h on HAp disks. ADSCs were cultured on FL, HC, PI and IS. Red = Phalloidin, Actin staining. Blue = DAPI, Nuclei, (b) Paxillin (green) immunofluorescent staining for ADSCs cultured for 24 h on HAp bioceramics surfaces FL, HC, PI, and IS. magnification is 60×. The insets represent the high magnification images of selected regions. (For interpretation of the references to color in this figure legend, the reader is referred to the Web version of this article.)

osteogenic differentiation. BMP-2 gene expression levels were significantly upregulated in ADSCs seeded on IS substrate, compared to the other substrates at day 14 (Fig. 7a). Further investigation into the expression of BMP-2 protein levels revealed a similar trend to the ones observed with the gene expression. IS substrates exhibited elevated levels of BMP-2 compared to the other HAp substrates (Fig. 7b).

4. Discussion

In this study, we developed and employed a low cost and facile method to create intricate bioinspired topographies onto HAp disks by casting of a ceramic slurry containing HAp nanoparticles on plant leaves. The topographies on leaves were replicated without detrimentally affecting the chemical composition of the underlying ceramic material. Furthermore, the complex structure of topographies remained intact during removing disks from molds, drying and sintering. This technique provides an excellent platform to create a range of complex patterns on ceramic substrates and identify optimized patterns suitable for inducing highly active cellular responses and the stimulatory effects. This technique has enabled us to explicitly explore complex topographies such as pillars, honeycomb or isolated islands on ceramic substrates. There is a large body of evidence that shows cells are influenced by symmetrical topographies (e.g. grooves, nanopores, spheres and cylinders) (Table 2). Most of these studies have been using metallic or organic substrates due to ease of fabrication.

The substrate topographies can be sensed by stem cells through a series of intracellular signalling and cascade amplification pathways, with topography being able to profoundly influence adhesion, proliferation, differentiation, and several cellular functions [38]. Generally, the specific mechanism of topography-driven stem cell differentiation remains unclear [38]. However, it is well-established that cells recognize the topographic cues, these cues are transmitted within cells and there is an interplay between topographic cues and chemical signals [39]. Many types of stem cells such as ADSCs are contractile cells and sense the micron and submicron scales topographies through contact guidance phenomenon which leads to the formation of lamellipodia and filopodia [40]. These two structures are both actin-based filament structures and immediately observed when cells are in contact with topographies. The topographical information is transmitted into cells through the maturation of the filaments into an adhesion structure, focal adhesion, which eventually leads to a specific cellular function [39,40]. Initial cues of molecular mechanisms by which cells sense a difference in topographies

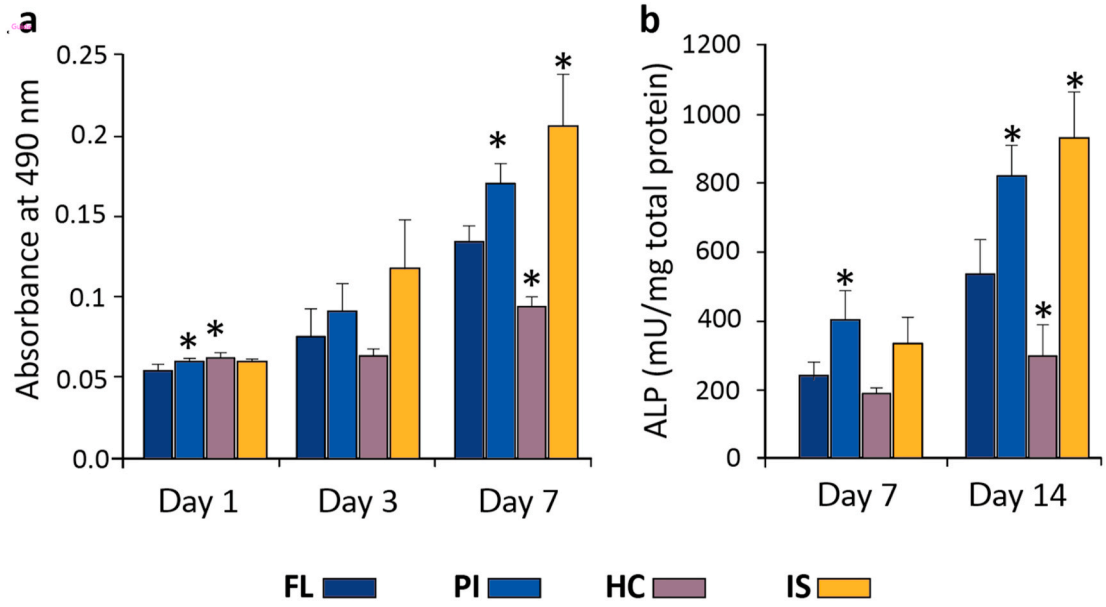

Fig. 5. (a) Proliferation of ADSCs cultured for 1, 3 and 7 days on HAp disks. (b) Osteogenic differentiation of ADSCs through the quantitative analysis of alkaline phosphatase activity after culturing the cells on HAp disks at day 7 and day 14 respectively.

are reflected in focal adhesion structures [41]. Variations of focal adhesion size, strength, and composition often reflect changes in actin contractility and point to Ras homolog family member A (RhoA), a small GTPase whose activation enhances non-muscle myosin IIa-dependent actin contractility by stimulating the formation of stress fibers and focal adhesions [42,43]. Several studies have demonstrated the critical role of RhoA, Rho-associated kinase (ROCK), and their downstream effects on actomyosin contractility on the regulation of cell fate by cell shape [44]. Generally, the consensus is that stem cells differentiate toward an osteogenic lineage when RhoA/ROCK pathway is activated which leads to cell spreading; whereas adipogenesis is dominated when cell spreading is restricted [45]. Another key regulator is focal adhesion kinase (FAK), generally regarded as upstream of RhoA activation and that is also influenced by changes in substrate nanotopography [46]. The focal adhesions also provide a physical link between integrins, a large family of transmembrane receptors, and topographic features. Some studies show the newly formed focal adhesions can phosphorylate FAK and FAK activity can directly affect the topography-induced gene expression [47]. Focal adhesion formation is directly influenced by different topographies. For example, nanopore arrays imprinted on a substrate tend to disrupt the formation of focal adhesions in osteoblasts [48]. Compared to flat substrates, substrates with 10 μm groove/ridge arrays hindered osteogenic differentiation but promoted adipose differentiation and formed less focal adhesions [47]. In contrast, a 100 μm groove/ridge could promote osteogenic differentiation of mesenchymal stem cells and promote focal adhesion formation. The Wnt pathway is a well-known canonical signalling pathway that modulates osteogenic differentiation and also closely related to cell cytoskeleton function [49]. Recent studies have shown that during the osteogenic differentiation of stem cells, surface topography and chemistry can affect the Wnt pathway [50]. Besides, the various topographies affect the cytoskeletal formation of cells through Wnt pathway. These surfaces have been made from a variety of materials including metals such as titanium alloys, inert polymers such as polydimethylsiloxane (PDMS) (Table 2). Though many studies demonstrated the impact of the surface topography on cell behaviour, these studies have utilized purely symmetrical geometries which do not recapitulate the complex geometries that are presented to cells *in vivo*. For instance, Pilia et al. investigated the influence of osteoblasts on the microgroove topographies imprinted on HAp surface with hemicylindrical shapes with 100 μm, 250 μm and 500 μm in diameter [51]. They observed that osteoblasts were able to orient and organize themselves alongside the axis of the grooves, upregulating key osteogenic markers such as alkaline phosphatase and osteopontin, compared to control unmodified flat surface. Dalby et al. demonstrated that microgroove topographies in the form of symmetrical hemicylinders with a diameter of 5 μm and 50 μm on HAp substrates regulate the migratory pattern of osteoprogenitor cells alongside the grooves [52]. Sia et al. showed that microgroove imprinted substrates consisting of channels of 10–20 μm in diameter on PDMS can reprogram fibroblasts into cardiomyocytes without the need for biochemical manipulations [53]. Recently, Werner et al. studied the migratory response of human bone marrow stromal cells to arrays of cylindrical PDMS topographies with a wide spectrum of diameter ranging from 250 to 1000 μm [54]. They demonstrated that cells on convex surfaces were elongated and aligned along the longitudinal axis of the cylinder with a pronounced effect when the cylinder diameter decreases. Park et al. studied the behaviour of human mesenchymal stem cells on PDMS substrate with hemisphere topographies with diameters of 200–300 μm and depth of 50–150 μm. They showed that stem cells actively escape from pits, whilst they attach and proliferate on protruded structures [55]. In our study, ADSCs responded with significant differences in cytoskeletal organizations and actin-extensions to non-symmetric and anisotropic topographies on HAp substrates. In ADSCs showed more actin filament extensions on IS (Fig. 4a) and distinguished cell attachment (Fig. 3), compared to HC, PI or the FL surfaces. Enhanced ADSCs response indicated that topography with isolated islands was able to facilitate enhanced cell-material interactions and provided better aspect ratio in terms of space, length, breadth and the curvature for the cells to attach, spread and form well-extended actin filaments. Paxillin, a focal adhesion-associated signal transduction adaptor proteins, is an intracellular protein confined to adhesion points on the inner cell surface and it is one of several adaptor proteins that connect integrins to the cytoskeleton [38,56]. ADSCs cultured on IS surfaces exhibited visible and strong paxillin aggregates on the substrates. These results suggest that the IS substrates induce favourable anchor points for the adhesion molecule as compared to the FL or PI surface and these paxillin aggregates were largely impaired on HC pattern (Fig. 4b). The inhomogeneous distribution of paxillin could be one of the reasons for decreased cell adhesion and spreading on the HC substrates. Tamiello et al. and Uttarayat et al. summarized that the groove dimension on PDMS

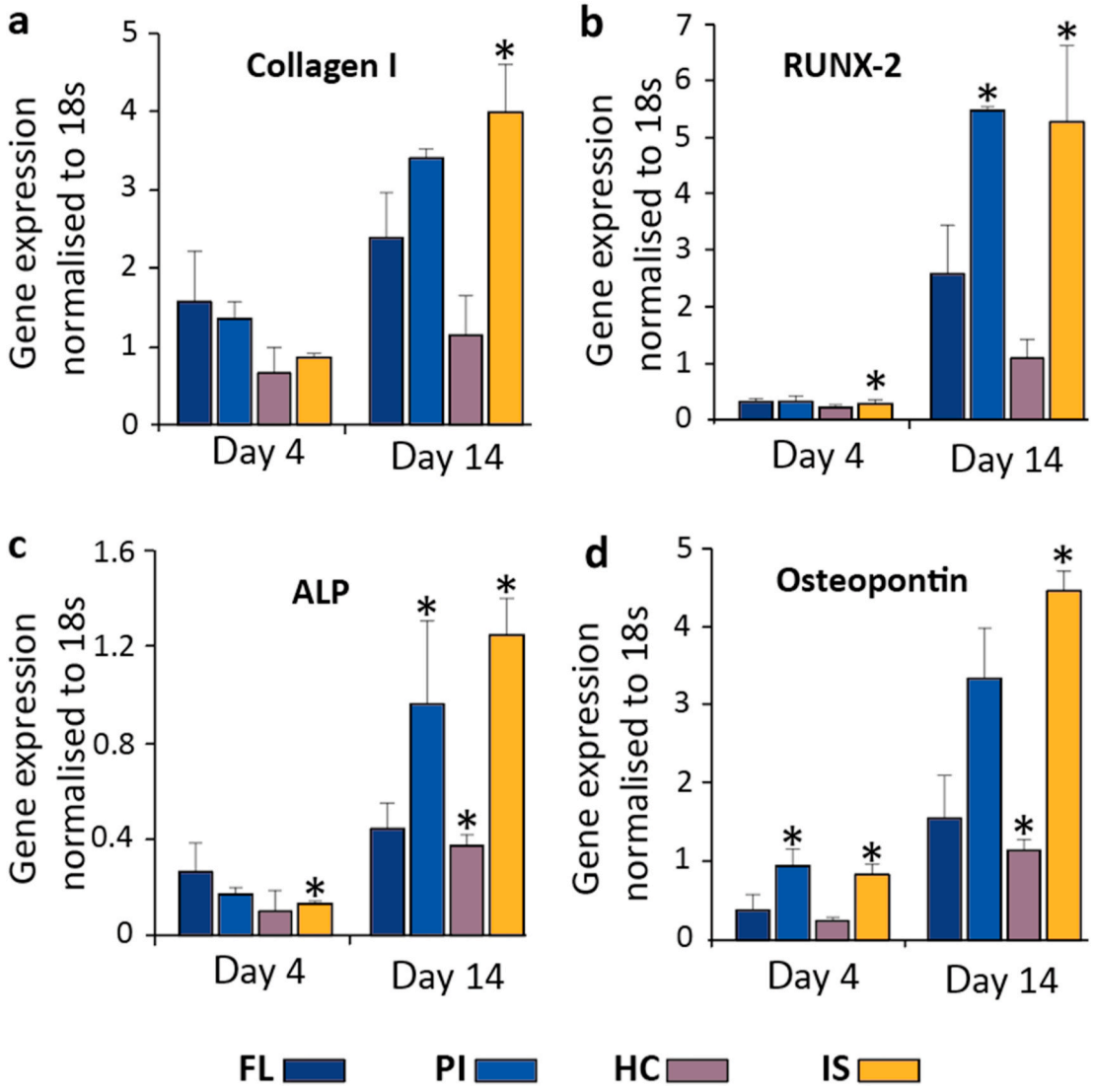

Fig. 6. Real-time PCR analysis of the expression of osteogenic genes (a) collagen I, (b)RUNX-2, (c)ALP and (d)osteopontin after culturing ADSCs at day 4 and day 14 on all the HAp disks. Results were standardised using 18 S as the housekeeping genes.

surfaces and anisotropic nature of a groove can significantly influence bovine endothelial cell responses [57,58]. It was observed that the majority of the focal adhesions and actin fibres of endothelial cells were oriented in the direction of the ridges and localised along the sidewalls of the grooves. The focal adhesions were explicitly expressed on the PDMS substrates with the groove depth of less than 1 μm and were absent on surfaces with grooves beyond 1 μm size. These versatile irregularities in cell morphology due to groove depth suggest that an environment which does not facilitate adhesion anchor points may be unfavourable for cell adhesion. In our study, the enhanced degree of paxillin clusters on IS and PI may have played a greater role in triggering increased ADSCs proliferation and cell growth compared to HC and FL substrates. Our study indicates that IS and PI patterns developed on HAp ceramics are conducible for promoting cell-biomaterials interaction as reflected in the enhanced cell attachment and growth respectively (Figs. 3 and 5a). Furthermore, the effect of micropatterns on the osteogenic differentiation of ADSCs was evaluated by ALP activity (Fig. 5b) and the expression of osteogenic markers such as COL1, Runx-2, ALP and OPN which play a vital role in bone metabolism (Fig. 6). ALP is an early osteogenic marker which plays a critical role in phosphate regulation [59]. It was found that ADSCs cultured on IS substrates promoted a significant increase in the ALP activity and the ALP gene expression compared to any other HAp substrates. Similarly, COL1 is known to be an early osteogenic marker necessary for bone matrix formation, whereas RUNX-2, the principal gene for bone formation, constitute a network of activities and molecular switches for bone development [60]. COL1 and RUNX-2 molecules were upregulated significantly on the IS substrates, compared to the other HAp substrates used in this study. A similar trend was observed for OPN, which is critical for matrix synthesis (Fig. 6). Our results suggest that micropattern features on IS surfaces promote ADSCs initial cell adhesion and in turn enhance osteogenic differentiation.

BMP-2 is a potent osteoinductive cytokine that is capable of inducing bone formation and osteogenesis and plays a vital role in cell adhesion and migration. BMP-2 controls osteoblast proliferation and differentiation through Smad to the nucleus [61]. Smad proteins play a critical role in mediating BMP-induced signals from the cell surface to the nucleus. We investigated the BMP-2 gene and protein expression by ADSCs in response to the micropattern features developed in this study (Fig. 7). ADSCs cultured on IS substrate for three days resulted in significant upregulation of BMP-2 gene and protein levels compared to FL control and other patterned HAp substrates investigated in this study. Our findings provide evidence that topographical features of IS may have the highest capacity to induce the activation of bone morphogenetic protein

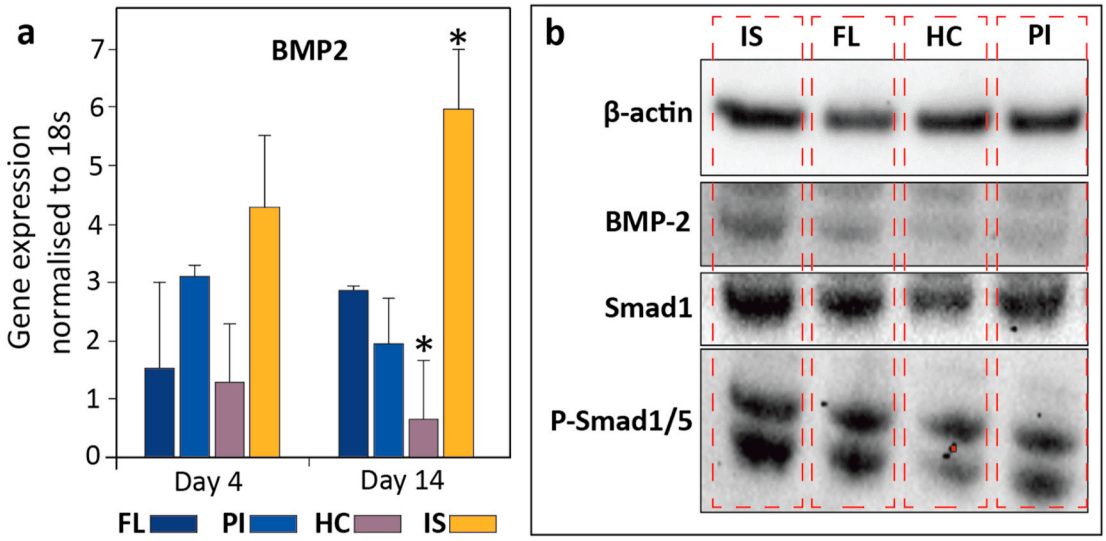

Fig. 7. (a) Real-time gene expression of BMP-2 from the ADSCs cultured on FL, PI, HC and IS at day 4 and day 14, and (b) the expression levels of BMP-2, Smad1 and phospho-Smad 1/5 (*P*-Smad 1/5) in ADSCs cultured on disks for three days. On (IS): Isolated islands, HC: honeycomb, PI: pillars. β-acting was used as the loading control.

Table 2
A summary of reports in the literature for topography-driven cell response: cytoskeleton organization and differentiation with respect to the shape and size of the topography.

Substrate material	Type of topography	Width/ diameter	Height	Cell type	Cell Response	Ref.
PMMA	Dot	140–2200 nm	11–45 nm	Human mesenchymal stem cells	Increased FA formation on nanodots, bone nodules formed on 45 nm high dots	[17]
Ti/TiO2	Dot	20–55.5 nm	30–115 nm	Human mesenchymal stem cells	Increased cytoskeleton organization, Focal adhesion size	[18]
PCL	Pit	20/30/40 μm	300 nm	Primary human osteoblasts	Increased cytoskeleton spreading and FA formation	[19]
PDMS coated	Pit	3 μm	2–4 μm	Murine mesenchymal stem cells	Increased FA size, actin polymerization and osteogenic differentiation	[20]
PMMA	Groove	10, 25, 100 μm	330 nm	Mesenchymal stem cells	Increased FA formation and osteoblastic differentiation	[21]
PC	Grooves	2 μm	7 μm	Osteoblasts	Decreased osteoblastic differentiation and FAs on grooved surfaces vs. flat surfaces	[22]
Ti	Groove	0.5–50 μm	1.3 μm	Mesenchymal stem cells	Increased cell attachment and spreading vs. flat surface. Larger cell adhesion density on narrower grooves (0.5 and 0.75 μm wide grooves)	[23]
Stainless steel	Groove	40, 50, 80 μm	~5–20 μm	Primary osteoblasts	Increased mineralization and alignment of collagen.	[24]
Polyimide	Microgroove	4 μm	5 μm	Osteoblasts	Strong elongation and alignment	[25]
PMMA	Nanogroove	10, 25, 100 μm	330 nm	Human osteoblasts	Decreased nanogroove widths led to increased contact guidance, decreased adhesion and increased angiogenic gene expressions	[26]
PS	Microgroove	1–10 μm	0.5–1.5 μm	Rat bone marrow cells	On large grooves, focal adhesions cover the surface,	[27]
PHBV	Microchannel	1–10 μm	5–30 μm	Rat mesenchymal stem cell-derived osteoblasts	Increased osteoblast adhesion and alignment	[28]
Collagen	Microchannel	27 μm	12 μm	Mesenchymal osteoprogenitor cells	Cell alignment facilitated enhanced bone formation	[29]
Collagen coated fibrinogen	Microgroove	27 μm	12 μm	Rat bone marrow osteoblast cells	Enhanced cell orientation and bone formation	[30]
PMMA	Micropillar	4, 8, 16 μm	8 μm	Dental pulm mesenchymal stem cells	8 μm height of the pillars showed enhanced osteogenic differentiation	[31]
PLGA	Micropillar	3 μm	7 μm	Mesenchymal stem cells	The geometry of cell nuclei responds to the micropillar array	[32]
PLGA	Micropillar	3 μm	5 μm	Bone marrow stromal cells	Reduced height showed severe nucleus deformation, but no change in proliferation and differentiation of bone marrow stromal cells	[33]
Ti	Micropillar	21 nm	15 nm	Bone marrow stromal cells	Improved bone deposition on nanopillars	[34]
PMMA	Nanopits	120 nm	100 nm	Mesenchymal stem cells	Stimulated differentiation and production of bone mineral in vitro	[35]
Ti	Micropits	100, 30, 10 μm		Osteoblast like cells	Cell attachment, growth, aggregation and morphology depends on the presence and dimension of the micropatterns	[36]
PCL	microwells	30 μm	80, 220, 333 nm	Bone marrow stromal cells	Optimal adhesion on 80 nm deep pits, inductive capability on 220 nm deep pits	[37]

PMMA: polymethylmethacrylate, PDMS: polydimethylsiloxane, PLLA: polylactic acid, PUA: polyurethane, PCL: polycaprolactone, PC: polycarbonate, PS: polystyrene, PLGA: polylactic glycolic acid. PS Polystyrene.

(BMP)/Smad pathway and in turn, osteogenic differentiation of ADSCs A similar observation was made by Zhao et al. who reported that both micro- and nanostructures could enhance cell-biomaterial interactions and promote cell behaviours via activating BMP-2 signalling pathway. Zhao et al. pointed out the correlation between integrins and BMP-2 signalling pathways and suggested that the osteogenic differentiation of bone marrow stromal cells induced by micro- and nanostructures could be attributed to the correlation between integrin-BMP-2 molecules [62]. It is therefore plausible to speculate that surface features of IS may have facilitated the initial adhesion of ADSCs extensively and thus stimulated the expression of the osteogenic markers to a greater extent and subsequently increasing its osteogenic potential compared to the other surfaces. One of the other factors is the influence of local surface curvature, which is independent of the size of topography. For example, Lin et al. [12], showed a "ridge-effect" where stem cells adhered on regions of highest mean curvature at the ridge of the elliptical cylinders progressively differentiated toward osteogenic lineage. This could be one of the reasons that cells on PI and IS showed an improved osteogenic differentiation where the average mean curvature of local topographies is higher than FL and HC substrates. It worth mentioning that degradation behaviour and mechanical properties are two important criteria for biomedical implants. The topographies are imprinted on the very surface of the substrate which will have a negligible effect on bulk mechanical properties. In case of topographies made from crystalline HAp, it is well-established that crystalline HAp (sintered at high temperature) is not degradable under physiological condition and HAp with a solid microstructure is stable even after long-term *in vivo* implantation [63].

5. Conclusion

In the present study, we developed a facile technique to replicate complex topographies found in plant surfaces onto the surface of HAp substrates. Plant-derived topographies are non-symmetric and anisotropic with hierarchical size scales which are challenging to fabricate by current manufacturing techniques. The simple fabrication method presented in this study can be used to develop intricate patterns on bioceramics to study and evaluate the optimal patterns for enhanced bone tissue regeneration and developing bioresponsive interfaces.

Declaration of competing interest

Authors declare no conflict of interest.

Acknowledgements

The authors acknowledge the Australia National Health and Medical Research Council, Australian Research Council, and the Rebecca L Cooper Medical Research Foundation. The authors acknowledge the Australian Research Council Training Centre for Innovative Bioengineering and the Australian Centre for Microscopy and Microanalysis (ACMM) at the University of Sydney for their help with microscopic analysis.

Appendix A. Supplementary data

Supplementary data to this article can be found online at https://doi.org/10.1016/j.bioactmat.2020.10.001.

References

[1] C. Zhao, L. Xia, D. Zhai, N. Zhang, J. Liu, B. Fang, J. Chang, K. Lin, Designing ordered micropatterned hydroxyapatite bioceramics to promote the growth and osteogenic differentiation of bone marrow stromal cells, J. Mater. Chem. B. 3 (2015) 968–976, https://doi.org/10.1039/C4TB01838A.

[2] M. Lasgorceix, C. Ott, L. Boilet, S. Hocquet, A. Leriche, M. Asadian, N. De Geyter, H. Declercq, V. Lardot, F. Cambier, Micropatterning of beta tricalcium phosphate bioceramic surfaces, by femtosecond laser, for bone marrow stem cells behavior assessment, Mater. Sci. Eng. C 95 (2019) 371–380.

[3] R.G. Carrodeguas, S. De Aza, α-Tricalcium phosphate: synthesis, properties and biomedical applications, Acta Biomater. 7 (2011) 3536–3546.

[4] D. Falconnet, G. Csucs, H.M. Grandin, M. Textor, Surface engineering approaches to micropattern surfaces for cell-based assays, Biomaterials 27 (2006) 3044–3063, https://doi.org/10.1016/j.biomaterials.2005.12.024.

[5] W. Bauer, J. Hausselt, Micropatterning of ceramics by slip pressing 25 (1999) 201–205.

[6] M.A. Lopez-Heredia, J. Sohier, C. Gaillard, S. Quillard, M. Dorget, P. Layrolle, Rapid prototyped porous titanium coated with calcium phosphate as a scaffold for bone tissue engineering, Biomaterials 29 (2008) 2608–2615, https://doi.org/10.1016/j.biomaterials.2008.02.021.

[7] L. Hu, Y. Zhang, S. Dong, S. Zhang, B. Li, In situ growth of hydroxyapatite on lamellar alumina scaffolds with aligned pore channels, Ceram. Int. 39 (2013) 6287–6291, https://doi.org/10.1016/j.ceramint.2013.01.050.

[8] I.S. Neira, Y. V Kolen'ko, O.I. Lebedev, G. Van Tendeloo, H.S. Gupta, F. Guitián, M. Yoshimura, An effective morphology control of hydroxyapatite crystals via hydrothermal synthesis, Cryst. Growth Des. 9 (2009) 466–474.

[9] S.Y. Chew, Y. Wen, Y. Dzenis, K.W. Leong, The role of electrospinning in the emerging field of nanomedicine, Curr. Pharmaceut. Des. 12 (2006) 4751–4770, https://doi.org/10.2174/138161206779026326.

[10] M.J. Dalby, N. Gadegaard, R. Tare, A. Andar, M.O. Riehle, P. Herzyk, C.D. W. Wilkinson, R.O.C. Oreffo, The control of human mesenchymal cell differentiation using nanoscale symmetry and disorder, Nat. Mater. 6 (2007).

[11] R.J. McMurray, N. Gadegaard, P.M. Tsimbouri, K. V Burgess, L.E. McNamara, R. Tare, K. Murawski, E. Kingham, R.O.C. Oreffo, M.J. Dalby, Nanoscale surfaces for the long-term maintenance of mesenchymal stem cell phenotype and multipotency, Nat. Mater. 10 (2011) 637–644.

[12] X. Lin, S. Romanazzo, K. Lin, C. Kelly, J.J. Gooding, I. Roohani, Elliptical supracellular topographies regulate stem cells migratory pattern and osteogenic differentiation, Materialia 14 (2020) 100870.

[13] P. Feng, M. Niu, C. Gao, S. Peng, C. Shuai, A novel two-step sintering for nano-hydroxyapatite scaffolds for bone tissue engineering, Sci. Rep. 4 (2014).

[14] C. Shuai, L. Yu, W. Yang, S. Peng, Y. Zhong, P. Feng, Phosphonic acid coupling agent modification of HAP nanoparticles: interfacial effects in PLLA/HAP bone scaffold, Polymers 12 (2020).

[15] S.-I. Roohani-Esfahani, S. Nouri-Khorasani, Z. Lu, R. Appleyard, H. Zreiqat, The influence hydroxyapatite nanoparticle shape and size on the properties of biphasic calcium phosphate scaffolds coated with hydroxyapatite-PCL composites, Biomaterials 31 (2010) 5498–5509.

[16] Y. Ramaswamy, C. Wu, A. Van Hummel, V. Combes, G. Grau, H. Zreiqat, The responses of osteoblasts, osteoclasts and endothelial cells to zirconium modified calcium-silicate-based ceramic, Biomaterials 29 (2008) 4392–4402, https://doi.org/10.1016/j.biomaterials.2008.08.006.

[17] M. John, D. Mccloy, M. Robertson, H. Agheli, D. Sutherland, S. Affrossman, R.O. C. Oreffo, Osteoprogenitor response to semi-ordered and random nanotopographies 27 (2006) 2980–2987, https://doi.org/10.1016/j.biomaterials.2006.01.010.

[18] T. Sjöström, M.J. Dalby, A. Hart, R. Tare, R.O.C. Oreffo, B. Su, Fabrication of pillar-like titania nanostructures on titanium and their interactions with human skeletal stem cells, Acta Biomater. 5 (2009) 1433–1441.

[19] A. Wilkinson, R.N. Hewitt, L.E. Mcnamara, D. Mccloy, R.M.D. Meek, M.J. Dalby, Acta biomaterialia biomimetic microtopography to enhance osteogenesis in vitro, Acta Biomater. 7 (2011) 2919–2925, https://doi.org/10.1016/j.actbio.2011.03.026.

[20] C.H. Seo, H. Jeong, Y. Feng, K. Montagne, T. Ushida, Y. Suzuki, K.S. Furukawa, Micropit surfaces designed for accelerating osteogenic differentiation of murine mesenchymal stem cells via enhancing focal adhesion and actin polymerization, Biomaterials 35 (2014) 2245–2252.

[21] M.J.P. Biggs, R.G. Richards, S. McFarlane, C.D.W. Wilkinson, R.O.C. Oreffo, M. J. Dalby, Adhesion formation of primary human osteoblasts and the functional response of mesenchymal stem cells to 330 nm deep microgrooves, J. R. Soc. Interface 5 (2008) 1231–1242.

[22] G. Kirmizidis, M.A. Birch, Microfabricated grooved substrates influence cell-cell communication and osteoblast differentiation in vitro, Tissue Eng. 15 (2009) 1427–1436.

[23] A.F. Cipriano, N. De Howitt, S.C. Gott, C. Miller, M.P. Rao, H. Liu, Bone marrow stromal cell adhesion and morphology on micro- and sub-micropatterned titanium, J. Biomed. Nanotechnol. 10 (2014) 660–668.

[24] A.C. De Luca, M. Zink, A. Weidt, S.G. Mayr, A.E. Markaki, Effect of microgrooved surface topography on osteoblast maturation and protein adsorption, J. Biomed. Mater. Res. 103 (2015) 2689–2700.

[25] J.L. Charest, L.E. Bryant, A.J. Garcia, W.P. King, Hot embossing for micropatterned cell substrates, Biomaterials 25 (2004) 4767–4775.

[26] R.L.R.D. Coutinho, P. Costa, N. Neves, M.E. Gomes, Micro and Nanotechnology in Tissue Engineering, Springer Berlin Heidelberg, Berlin, 2011.

[27] K. Matsuzaka, X.F. Walboomers, J.E. De Ruijter, J.A. Jansen, The effect of poly-L-lactic acid with parallel surface micro on groove on osteoblast-like cells in vitro, Biomaterials 20 (1999) 1293–1301.

[28] H. Kenar, A. Kocabas, A. Aydinli, V. Hasirci, Chemical and topographical modification of PHBV surface to promote osteoblast alignment and confinement, J. Biomed. Mater. Res. 85 (2008) 1001–1010.

[29] N.E. Vrana, A. Elsheikh, N. Builles, O. Damour, V. Hasirci, Effect of human corneal keratocytes and retinal pigment epithelial cells on the mechanical properties of micropatterned collagen films, Biomaterials 28 (2007) 4303–4310.

[30] S. Ber, G. Torun Köse, V. Hasirci, Bone tissue engineering on patterned collagen films: an in vitro study, Biomaterials 26 (2005) 1977–1986.
[31] O. Hasturk, A. Sivas, B. Karasozen, U. Demirci, N. Hasirci, V. Hasirci, Quantification of type, timing, and extent of cell body and nucleus deformations caused by the dimensions and hydrophilicity of square prism micropillars, Adv. Healthc. Mater. 5 (2016) 2972–2982.
[32] X. Liu, R. Liu, Y. Gu, J. Ding, Nonmonotonic self-deformation of cell Nuclei on topological surfaces with micropillar array, ACS Appl. Mater. Interfaces 9 (2017) 18521–18530.
[33] Z. Pan, C. Yan, R. Peng, Y. Zhao, Y. He, J. Ding, Control of cell nucleus shapes via micropillar patterns, Biomaterials 33 (2012) 1730–1735.
[34] R.K. Silverwood, P.G. Fairhurst, T. Sjöström, F. Welsh, Y. Sun, G. Li, B. Yu, P. S. Young, B. Su, R.M.D. Meek, M.J. Dalby, P.M. Tsimbouri, Analysis of osteoclastogenesis/osteoblastogenesis on nanotopographical titania surfaces, Adv. Healthc. Mater. 5 (2016) 947–955.
[35] E. Martínez, E. Engel, J.A. Planell, J. Samitier, Effects of artificial micro- and nano-structured surfaces on cell behaviour, Ann. Anat. 191 (2009) 126–135.
[36] O. Zinger, G. Zhao, Z. Schwartz, J. Simpson, M. Wieland, D. Landolt, B. Boyan, Differential regulation of osteoblasts by substrate microstructural features, Biomaterials 26 (2005) 1837–1847.
[37] M.J. Davison, R.J. McMurray, C.-A. Smith, M.J. Dalby, R.M.D. Meek, Nanopit-induced osteoprogenitor cell differentiation: the effect of nanopit depth, J. Tissue Eng. 7 (2016).
[38] J. Huang, Y. Chen, C. Tang, Y. Fei, H. Wu, D. Ruan, M.E. Paul, X. Chen, Z. Yin, B. C. Heng, W. Chen, W. Shen, The relationship between substrate topography and stem cell differentiation in the musculoskeletal system, Cell. Mol. Life Sci. 76 (2019) 505–521.
[39] S. Gerecht, C.J. Bettinger, Z. Zhang, J.T. Borenstein, G. Vunjak-Novakovic, R. Langer, The effect of actin disrupting agents on contact guidance of human embryonic stem cells, Biomaterials 28 (2007) 4068–4077.
[40] S. Lenhert, M.-B. Meier, U. Meyer, L. Chi, H.P. Wiesmann, Osteoblast alignment, elongation and migration on grooved polystyrene surfaces patterned by Langmuir-Blodgett lithography, Biomaterials 26 (2005) 563–570.
[41] J. Albuschies, V. Vogel, The role of filopodia in the recognition of nanotopographies, Sci. Rep. 3 (2013).
[42] A. Hall, Rho GTpases and the actin cytoskeleton, Science 279 (80) (1998) 509–514.
[43] G. Li, Y. Song, M. Shi, Y. Du, W. Wang, Y. Zhang, Mechanisms of Cdc42-mediated rat MSC differentiation on micro/nano-textured topography, Acta Biomater. 49 (2017) 235–246.
[44] M. Chiquet, L. Gelman, R. Lutz, S. Maier, From mechanotransduction to extracellular matrix gene expression in fibroblasts, Biochim. Biophys. Acta Mol. Cell Res. 1793 (2009) 911–920.
[45] K. a Kilian, B. Bugarija, B.T. Lahn, M. Mrksich, Geometric cues for directing the differentiation of mesenchymal stem cells, Proc. Natl. Acad. Sci. U.S.A. 107 (2010) 4872–4877.
[46] B.K.K. Teo, S.T. Wong, C.K. Lim, T.Y.S. Kung, C.H. Yap, Y. Ramagopal, L.H. Romer, E.K.F. Yim, Nanotopography modulates mechanotransduction of stem cells and induces differentiation through focal adhesion kinase, ACS Nano 7 (2013) 4785–4798.
[47] J.W. Cassidy, J.N. Roberts, C.-A. Smith, M. Robertson, K. White, M.J. Biggs, R.O. C. Oreffo, M.J. Dalby, Osteogenic lineage restriction by osteoprogenitors cultured on nanometric grooved surfaces: the role of focal adhesion maturation, Acta Biomater. 10 (2014) 651–660.
[48] M.J.P. Biggs, R.G. Richards, N. Gadegaard, C.D.W. Wilkinson, R.O.C. Oreffo, M. J. Dalby, The use of nanoscale topography to modulate the dynamics of adhesion formation in primary osteoblasts and ERK/MAPK signalling in STRO-1+ enriched skeletal stem cells, Biomaterials 30 (2009) 5094–5103.
[49] M.R. Byun, J.-H. Hwang, A.R. Kim, K.M. Kim, E.S. Hwang, M.B. Yaffe, J.-H. Hong, Canonical Wnt signalling activates TAZ through PP1A during osteogenic differentiation, Cell Death Differ. 21 (2014) 854–863.
[50] C. Galli, M. Piemontese, S. Lumetti, E. Manfredi, G.M. MacAluso, G. Passeri, The importance of WNT pathways for bone metabolism and their regulation by implant topography, Eur. Cell. Mater. 24 (2012) 46–59.
[51] M. Pilia, T. Guda, S.M. Shiels, M.R. Appleford, Influence of substrate curvature on osteoblast orientation and extracellular matrix deposition, J. Biol. Eng. 7 (2013) 1.
[52] M.J. Dalby, D. McCloy, M. Robertson, C.D.W. Wilkinson, R.O.C. Oreffo, Osteoprogenitor response to defined topographies with nanoscale depths, Biomaterials 27 (2006) 1306–1315, https://doi.org/10.1016/j.biomaterials.2005.08.028.
[53] J. Sia, P. Yu, D. Srivastava, S. Li, Effect of biophysical cues on reprogramming to cardiomyocytes, Biomaterials 103 (2016) 1–11.
[54] M. Werner, A. Petersen, N.A. Kurniawan, C.V.C. Bouten, Cell-Perceived substrate curvature dynamically coordinates the direction , speed , and persistence of stromal cell migration, Adv. Biosys. 3 (2019) 1–11.
[55] J.Y. Park, D.H. Lee, E.J. Lee, S.H. Lee, Study of cellular behaviors on concave and convex microstructures fabricated from elastic PDMS membranes, Lab Chip 9 (2009) 2043–2049.
[56] M.D. Schaller, Paxillin: a focal adhesion-associated adaptor protein, Oncogene 20 (2001) 6459–6472.
[57] C. Tamiello, A.B.C. Buskermolen, F.P.T. Baaijens, J.L. V Broers, C.V.C. Bouten, Heading in the right direction: understanding cellular orientation responses to complex biophysical environments, Cell. Mol. Bioeng. 9 (2016) 12–37.
[58] C. Tamiello, C.V.C. Bouten, F.P.T. Baaijens, Competition between cap and basal actin fiber orientation in cells subjected to contact guidance and cyclic strain, Sci. Rep. 5 (2015) 8752.
[59] T.T. Hlaing, J.E. Compston, Biochemical markers of bone turnover - uses and limitations, Ann. Clin. Biochem. 51 (2014) 189–202.
[60] J.H. Xu, Z.H. Li, Y.D. Hou, W.J. Fang, Potential mechanisms underlying the Runx 2 induced osteogenesis of bone marrow mesenchymal stem cells, Am. J. Transl. Res. 7 (2015) 2527–2535.
[61] Y. Yoshida, S. Tanaka, H. Umemori, O. Minowa, M. Usui, N. Ikematsu, E. Hosoda, T. Imamura, J. Kuno, T. Yamashita, K. Miyazono, M. Noda, T. Noda, T. Yamamoto, Negative regulation of BMP/Smad signaling by Tob in osteoblasts, Cell 103 (2000) 1085–1097.
[62] C. Zhao, X. Wang, L. Gao, L. Jing, Q. Zhou, J. Chang, The role of the micro-pattern and nano-topography of hydroxyapatite bioceramics on stimulating osteogenic differentiation of mesenchymal stem cells, 2018, https://doi.org/10.1016/j.actbio.2018.04.030.
[63] K. Lin, R. Sheikh, S. Romanazzo, I. Roohani, 3D printing of bioceramic scaffolds-barriers to the clinical translation: from promise to reality, and future perspectives, Materials 12 (2019) 2660.